2022 44th Annual International Conference of
the IEEE Engineering in Medicine & Biology Society (EMBC)
Scottish Event Campus, Glasgow, UK, July 11-15, 2022

2022 44th Annual International Conference of the IEEE Engineering in Medicine & Biology Society (EMBC) | 978-1-7281-2782-8/22/$31.00 ©2022 IEEE | DOI: 10.1109/EMBC48229.2022.9871005

Development and Characterization of Passivation Methods for Microneedle-based Biosensors

Andrea Bocchino, Sofia Rodrigues Teixeira, Simone Iadanza, Eva Melnik, Steffen Kurzhals, Giorgio C. Mutinati, and Conor O'Mahony, *Senior Member, IEEE*

Abstract— **Microneedles (MN) are short, sharp structures that have the ability to painlessly pierce the *stratum corneum*, the outermost layer of the skin, and interface with the dermal interstitial fluid that lies beneath. Because the interstitial fluid is rich in biomarkers, microneedle-based biosensors have the potential to be used in a wide range of diagnostic applications. To act as an electrochemical sensor, the tip or the body of the MN must be functionalized, while the substrate areas are generally passivated to block any unwanted background interference that may occur outside of the skin. This work presents four different passivation techniques, based on the application of SiO_2, polymethyl methacrylate (PMMA), an adhesive film, and varnish to the substrate areas. Optical, SEM and electrochemical measurements were performed to quantitatively assess the performance of each film. The data shows that whilst manual application of varnish provided the highest level of electrical isolation, the spin-coating of a 5 μm thick layer of PMMA is likely to provide the best combination of performance and manufacturability.**

Clinical Relevance— **Substrate passivation techniques will improve the performance of microneedle-based non-invasive continuous monitoring systems.**

I. Introduction

Molecular biomarkers are widely used for the diagnosis and monitoring of a myriad of conditions ranging from diabetes and cardiology to athletic performance and nutritional health [1]. Biomarkers are usually analysed from either saliva or blood samples, and while saliva samples are convenient to collect, not all saliva-borne biomarkers are correlated to their corresponding levels in blood samples [2]. Furthermore, the inconvenient and invasive nature of blood sampling techniques means that frequent biomarker monitoring using this method has limited appeal [3].

In contrast, dermal interstitial fluid (ISF), i.e. the extracellular fluid that surrounds the cells in the uppermost skin layers, is easily accessible and its biomarker profiles show good correlation with those found in blood. As a result, microneedle-based technologies are receiving significant attention as a method of sampling interstitial fluid-borne biomarkers. MNs are short, sharp projections that painlessly penetrate the skins outermost *stratum corneum* layer, interface with the underlying epidermis and, because their length is generally less than 1 mm, the use of microneedle-based sensors does not strike nerve endings or blood vessels. Their application is therefore perceived as painless by the user [4].

While several teams have proposed the use of hollow microneedles to remove small volumes of ISF for subsequent analysis, an alternative technique is to perform continuous *in-situ* monitoring, using microneedle arrays on which electrochemical sensing capabilities have been placed at or near the needle tip. Using this approach, microneedle-based devices have been investigated as minimally invasive sensors mainly for transdermal lactate and glucose diagnostics [4, 5].

In the EU H2020 project "Electronic smart patch system for wireless monitoring of molecular biomarkers for healthcare and well-being (ELSAH)", we are developing MN-based biosensors that will be integrated with flexible power sources, ASIC conditioning circuitry, wireless communications and printed antennae to form a wearable patch for applications in simultaneous glucose and lactate monitoring [6].

In a similar approach to that used by others, needle tip functionalisation will be achieved by depositing biocompatible polymeric materials and biomarker-specific chemistries over the arrays, and because it is often challenging to precisely deposit and pattern these layers on the steep sidewalls and micron-scale tips associated with microneedle structures, undesirable functionalisation of the substrate may also take place. Therefore, after array metallization, the substrate areas that are not used for sensing should be electrically isolated or 'passivated' to block any undesired response that may occur outside of the skin. Commonly used

*This work was funded by the European Union's Horizon 2020 research and innovation programme under grant #825549 (ELSAH project).

A. Bocchino is with Tyndall National Institute, University College Cork, Ireland (andrea.bocchino@tyndall.ie).

S. Teixeira is with Tyndall National Institute, University College Cork, Ireland (sofia.teixeira@tyndall.ie).

S. Iadanza is with Tyndall National Institute, University College Cork and Munster Technological University, Ireland (simone.iadanza@mtu.ie).

E. Melnik is with AIT Austrian Institute of Technology GmbH, Center for Health and Bioresources, Molecular Diagnostics, Giefinggasse, 4, 1210 Vienna, Austria (eva.melnik@ait.ac.at).

S. Kurzhals is with AIT Austrian Institute of Technology GmbH, Center for Health and Bioresources, Molecular Diagnostics, Giefinggasse, 4, 1210 Vienna, Austria (steffen.kurzhals@ait.ac.at).

G. Mutinati is with AIT Austrian Institute of Technology GmbH, Center for Health and Bioresources, Molecular Diagnostics, Giefinggasse, 4, 1210 Vienna, Austria (giorgio.mutinati@ait.ac.at).

C. O'Mahony is with Tyndall National Institute, University College Cork, Ireland (conor.omahony@tyndall.ie).

passivation techniques include chemical vapour deposition (CVD) [7] or plasma-enhanced CVD (PECVD) [8], spin coating [5], oxide layer formation [9] or manual application of insulating varnish [10].

Although microneedle array passivation is widely used in interstitial diagnostics, there is little to no data regarding passivation layer characterization. In this paper, we firstly develop a polymer-based biosensor substrate, before using a range of scalable and manual techniques to deposit passivation layers using silicon oxide (SiO_2), varnish, PMMA, and a commercially available adhesive film. With a goal of minimising film thickness whilst maximising the electrical isolation of the substrate, we then use microscopy and electrochemical analysis to assess and compare the performance of each material and deposition approach.

The results show that the application of the varnish provided the highest level of electrical isolation, while the spin coating of a 5µm thick layer of PMMA, that gave the second lowest peak-to-peak currents, is likely to provide the best combination of performance and manufacturability.

II. Materials and Methods

A. Microneedle Array Production

Polymer MN arrays were produced using a replica moulding process (Fig. 1) [11], starting from a front side master template. The template is comprised of a 100 mm diameter silicon wafer attached to a glass petri dish. 500 µm tall silicon MNs were etched on the wafer prior to attachment.

A back side master was also produced using a PVC petri dish into which a custom geometry was milled. This master was intended to divide the moulded wafer into detachable individual arrays. PDMS (Sylgard 184, Dow Corning, MI, USA) was poured on both masters, degassed, cured and then peeled off to obtain a front (Fig. 1A) and a back (Fig. 1B) mould. The two components of Epotek 353ND (Epoxy Technology, MA, USA), a medical-grade epoxy, were mixed according to manufacturer's instructions, poured on top of the front mould and degassed in a vacuum chamber. The back mould was consequently positioned on the front mould, sandwiching the polymer in between.

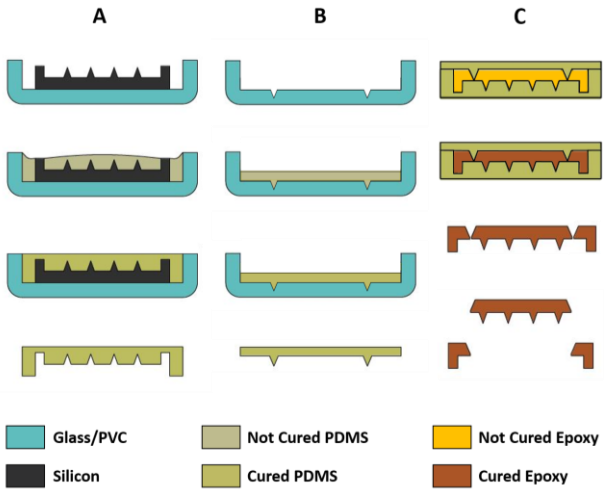

Figure 1. Replica moulding process for MNs production: front (A) and back (B) moulds are manufactured from the master substrates and used to produce polymer wafer with detachable MN arrays (C).

The stack was then placed on a vacuum table to ensure proper filling of the MN holes. Finally, the polymer was thermally cured and both moulds peeled away, resulting in a 100 mm diameter polymeric wafer, divided into individual arrays corresponding to the shape of the back side (Fig. 1C).

The polymeric wafer was then metallized on the front and back surfaces by sputtering 20 nm of titanium (Ti) and 100 nm of platinum (Pt). The division provided by the back mould allowed front to back electrical connection on the individual arrays. On the wafer, the single arrays used in this work were designed as circles with a diameter of 9 mm, on which MNs were arrayed at a pitch of 1.75 mm, Fig. 2.

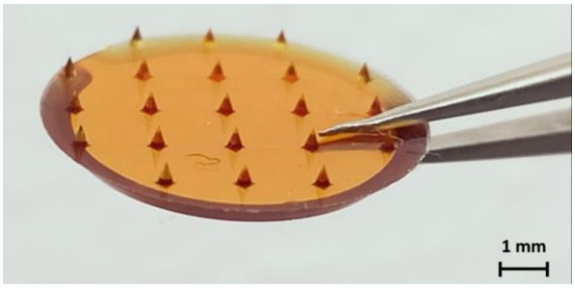

Figure 2. Picture of a 9 mm MN array before metallization.

B. Microneedle Array Passivation

Four different passivation techniques have been used in this work: sputtering of SiO_2; application of an adhesive film; direct brushing of nail varnish and spin-coating of PMMA.

For SiO_2 deposition and patterning, a metal shadow mask was fabricated using vertical machining centers (VMC) machining and attached to the MN wafer. The mask was composed of 1 mm wide metal strips alternating with 0.75 mm wide openings. The mask was aligned so that the strips covered each row of MNs. After sputtering, the mask was then detached, rotated 90° and re-attached to the wafer to cover the MNs lying along the perpendicular axis. After a second sputtering process, the SiO_2 was deposited between each horizontal and vertical row of microneedles, leaving only an exposed square of 1 x 1 mm^2 around each needle. A 300 nm thick oxide layer was deposited during each deposition.

For the adhesive film application, ARcare 7759, a 55 µm thick medical-grade tape from Adhesives Research (Limerick, Ireland), was cut using a Graphtec CE7000-40 vinyl cutter. The tape was shaped in circles with a diameter of 9.5 mm, into which 500 µm circular holes were cut at a pitch that corresponded to that of the MNs. The tape was then aligned with the MNs and attached to the array. Pressure was manually applied to the tape, pressing with tweezers in between the MNs, to ensure proper attachment to the substrate.

The varnish, Maybelline 130 from Maybelline (New York, USA), was directly brushed over the individual arrays. The liquid flowed towards the base of the needles due to gravity, exposing the tip of the MNs. After the first layer of varnish had dried, the process was repeated a second time.

An OPTIcoat ST30 spin coater from ATMvision (Singen, Germany) was used to cover the arrays with a 5 µm layer of A15 PMMA from EM Resist (Manchester, England). After covering, the arrays were placed in a covered hot plate and baked at 150°C for 5 minutes to cure the PMMA.

C. Microneedle Testing

After passivation, all samples were analyzed using an optical microscope and a Zeiss Supra 40 scanning electron microscope (SEM) to verify the percentage of the MNs that was covered by each passivation layer and to visually estimate the area available for electrochemical functionalization.

In order to quantitatively evaluate and compare the different passivation methods, an electrochemical assessment was performed. 3D printed supports were produced and provided with an electrical connection. Each MN array was glued using Epotek H20E (Epoxy Technology, MA, USA) to one of these supports. Loctite Power Flex superglue (Henkel Corp., OH, USA) was used to completely seal any possible gap between the support and the array.

Finally, the MN arrays were analyzed using cyclic voltammetry (CV). All electrochemical measurements were carried out with an Autolab MAC90389 electrochemical workstation (Metrohm, Cheshire, UK) using NOVA 2.1 software. All experiments were performed at room temperature using a Faraday cage (Metrohm). CV measurements were carried out using the microneedle array as working electrode (WE), an Ag/AgCl reference electrode (RE) (Gamry, Warminster, PA 18974, USA) and a Pt wire (Gamry Instruments, PA, USA) as a counter reference (CE).

Phosphate buffered saline, ferrocenemonocarboxylic acid, ammonium chloride and hydrogen peroxide (30%) were purchased from Sigma Aldrich (Arklow, Ireland). All solutions were prepared using deionized Milli-Q water (resistivity 18.2 MΩ.cm).

The microneedle array was characterised using CV in a 10 mM phosphate buffered solution (PBS; pH = 7.4) containing 1 mM ferrocenemonocarboxylic acid (FcCOOH). CV was performed by cycling the potential from 0 V to 0.6 V at a scan rate of 0.15 V/s. A cleaning step was performed before and after each characterization step using CV in a 5:1:1 ratio of H_2O: ammonium chloride: hydrogen peroxide (H_2O_2), and the CV was performed by cycling the potential from -0.5 V to 0.5 V at a scan rate of 0.15 V/s versus the Ag/AgCl RE and the Pt wire CE.

III. Results

After optical microscope and SEM imaging, image analysis was performed using ImageJ to calculate the unprotected area for each microneedle array. The microscope images were also used to detect substrate areas that were imperfectly passivated. SEM pictures were used to estimate the non-passivated surface of the MNs: a fully passivated array was imaged and 6 MNs were measured to calculate the average exposed area. This average was then used to estimate the unprotected area on each similarly passivated device. Fig. 3 shows the MN arrays passivated using ARcare, PMMA and varnish, compared with a bare microneedle used as a control. SEM pictures were taken also for the sample covered with SiO_2 however, there was no evident visual difference between the passivated needle and the control needle. Therefore, the image was not included.

The MNs used in this study have the shape of an octagonal pyramid. The following formulas were used to calculate the lateral surface area, A_l and the base area A_b, of the pyramid:

$$A_l = 2s\sqrt{4h^2 + s^2 cot^2\left(\frac{\pi}{8}\right)} \quad (1)$$

$$A_b = 2s^2 cot\left(\frac{\pi}{8}\right) \quad (2)$$

where s is the base edge length and h is the pyramid height.

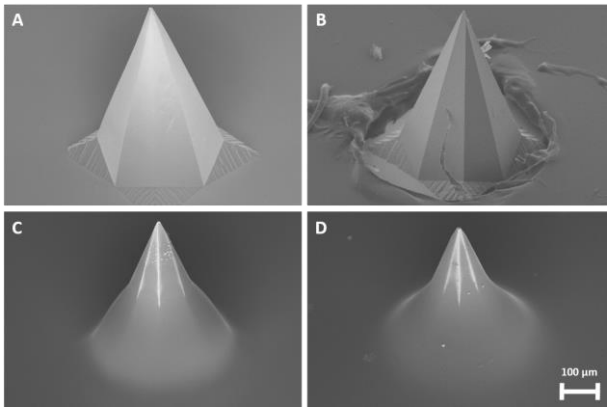

Figure 3. SEM image of a non-passivated MN (A) and MN passivated using ARcare tape (B), PMMA (C) and varnish (D) respectively. All microneedles have a nominal height of 500 µm.

From the SEM pictures the surface area of an uncoated MN was calculated to be 0.259 mm^2 (h = 500 µm, s = 124 µm) while the base area was 0.074 mm^2. The surface areas of the exposed region for the passivated microneedles were 0.076 mm^2 (h = 263 µm, s = 69 µm) and 0.06 mm^2 (h = 240 µm, s = 60 µm) for the varnish and PMMA covered MNs, respectively. For the ARcare passivation method, the MNs were considered fully exposed, together with a circular substrate area of 0.5 mm diameter around them. Similarly, the SiO_2 passivation method was considered to leave the MNs entirely exposed together with a substrate square of 1mm^2 with the needle in the centre. In both cases, when calculating the area of the non-passivated surface, the base of the MNs was subtracted from the exposed area around the needles. The estimated non-passivated area ranged from 54.6 mm^2 for the control array, to 15.66 mm^2 using SiO_2, 8.13 mm^2 using ARcare, 1.12 mm^2 using PMMA and 1.52 mm^2 using varnish.

In order to assess the electrical isolation provided by each passivation technique, cyclic voltammetry was carried out in a 1 mM FcCOOH redox probe to electrochemically characterise the modified MN array surface with a three-electrode set-up. Higher currents imply that the layer under test was less successful at providing electrochemical isolation than the ones with lower values. Results of electron transfer behaviour are summarized in Fig. 4. Peak potential (both for oxidation and reduction processes, namely E_{ox} and E_{red}), peak current (both for oxidation and reduction processes namely I_p^{ox} and I_p^{red}) and half-wave potential values ($E_{1/2}$) were all extracted from the graph and can be seen in Table I. The used scan rate was 150 mV/s.

The respective E_{ox} and E_{red} values for the control electrode were determined to be 337mV and 25 mV along with an $E_{1/2}$ value of 81mV. Similarly, the corresponding I_p^{ox} and I_p^{red} values was found to be 8.08×10^{-5}A and -5.86×10^{-5}A. Comparing with the control, the $E_{1/2}$ value of the redox couple on the SiO_2 electrode was found to be lower (41mV). Similarly, E_{ox} value was found to be lower (327mV) while

measured E_{red} values higher (286mV). On the other hand, for ARcare passivated electrodes, an $E_{1/2}$ value of 70mV is determined. The corresponding E_{ox} and E_{red} values along with I_p^{ox} and I_p^{red} values are shown in Table I. An increase in both E_{ox} and E_{red} is visible in the case of the PMMA and Varnish with a decrease in both I_p^{ox} and I_p^{red} values.

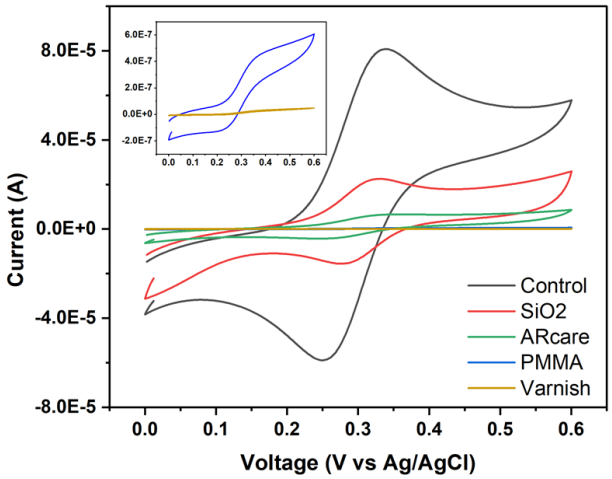

Figure 4. Cyclic voltammetry scans performed at each passivated surface in 1 mM FcCOOH in 10 mM PBS.

TABLE I. Peak potential values (Oxidation - E_{ox}; Reduction - E_{red}), peak current values (Oxidation - I_p^{ox}; Reduction - I_p^{red}) and half-wave potential values ($E_{1/2}$) at a scan rate of 150mV/s obtained from the recorded CV curves.

Passivation	Peak Potential (mV)		Peak Current (x 10^{-6} A)		$E_{1/2}$ (mV)
	E_{ox}	E_{red}	I_p^{ox}	I_p^{red}	/
Control	337	256	80.8	-58.6	81
SiO_2	327	286	26.2	-17.7	41
ARcare	329	259	6.30	-4.20	70
PMMA	359	249	0.43	-0.87	110
Varnish	361	268	0.029	-0.002	93

IV. Conclusion

As expected, the passivation methods reduced the area available for surface modification, leading to lower observed currents. Smaller exposed areas led to lower currents, with the exception of the varnish technique: although the estimated unprotected area was around 35% bigger than the one left by PMMA coating, the voltammetry results showed currents one order of magnitude lower when varnish was used. Additional optical microscope inspection showed that a thin layer of varnish close to the tip of the MNs was not detectable with the SEM, but was optically evident due to the colour of the varnish. Therefore, the effective exposed area obtained after varnish application was smaller than that originally estimated using SEM (1.52mm^2), leading to lower currents, Fig. 4.

The varnish showed the lowest currents. However, reflecting the manual nature of the application method, it also showed significant coverage variation from needle to needle. PMMA was the second-best result in terms of current reduction but showed more uniform and predictable protection of the needles, and the semiconductor-based nature of the wafer fabrication and spin coating approach means that this is easily scalable to high volumes and in industrial settings. SiO_2 deposition is also a highly scalable technique but it resulted in a moderately successful passivation: the clearance in between shadow mask and MNs, necessary to prevent damages to the needle tips, allowed diffraction of the oxide underneath the mask, compromising the precision of the technique. Moreover, the adhesion of the oxide to the surface was weaker than any other technique: simply cleaning the arrays was causing oxide detachment. The passivation obtained using the ARcare tape showed a reduction of the currents but the necessity to leave some clearance around the MN and the precision constraints of the cutting machine, limited this technique from fully covering the base of the arrays. However, this is the more mechanically robust passivation layer and, if required, could also be used in development of flexible sensors. In addition, using double-sided tape instead of single-faced tape, could help improving skin adhesion of wearable devices.

The study shows that the deposition of passivation layers for microneedle-based biosensors is feasible using a range of materials and application techniques, and that these may be quantitatively characterised using optical and electrochemical techniques. Of the different layers tested in this work, the most promising one is PMMA, which combines good performance with quick and reproducible manufacturability. Ongoing work is being carried out for the functionalisation of the microneedle tips for applications in glucose and lactate monitoring.

Acknowledgment

The authors would like to acknowledge Shane O'Sullivan for cutting tape samples and Tyndall Specialty Products and Services team for the fabrication of silicon master templates.

References

[1] R. Liu, "Recent progress of biomarker detection sensors", *AAAS Research*, Volume 2020, 7949037, October 2020.

[2] S. Williamson, "Comparison of biomarkers in blood and saliva in healthy adults", *Nursing Research and Practice*, Hindawi Publishing Corporation, Volume 2012, 246178.

[3] B. U. W. Lei, "A review of microsampling techniques and their social impact", *Biomedical Microdevices*, vol. 21, 81, August 2019.

[4] J. Madden, "Biosensing in dermal interstitial fluid using microneedle based electrochemical device", *Sensing and Bio-Sensing Research*, vol. 29, 100348, August 2020.

[5] C. Barrett, "Development of low cost rapid fabrication of sharp polymer microneedles for in vivo glucose biosensing applications", *ECS Journal of Solid State Science and Technology*, 4 (10) S3053-S3058, August 2015.

[6] H2020 ELSAH project website, www.elsah.researchproject.at, accessed 24.01.2022.

[7] A. T. Satti, "Fabrication of Parylene-coated microneedle array electrode for wearable ECG device", *Sensors*, 20, 5183, September 2020.

[8] J. Held, "Microneedle array for intracellular recording applications", *MEMS 2008*, Tucson, AZ, USA, 13-17 January 2008.

[9] W.-C. Lee, "Microneedle array sensor for monitoring glucose in single cell using glucose oxidase-bonded polyterthiophene coated on AuZn oxide layer", *Sensors and Actuators B: Chemical*, vol. 320, 128416, October 2020.

[10] S. A. N. Gowers, "Development of a minimally invasive microneedle-based sensor for continuous monitoring of β-lactam antibiotic concentrations in vivo", *ACS Sensors*, 4, 4, 1072-1080, April 2019.

[11] C. O'Mahony, "Design, fabrication and skin-electrode contact analysis of polymer microneedle-based ECG electrodes" *Journal of Micromechanics and Microengineering*, vol. 26, p.084005, July 2016.